



Asymmetry underlies stability in power grids

Ferenc Molnar^{1,3}, Takashi Nishikawa^{1,2}   & Adilson E. Motter^{1,2} 

Behavioral homogeneity is often critical for the functioning of network systems of interacting entities. In power grids, whose stable operation requires generator frequencies to be synchronized—and thus homogeneous—across the network, previous work suggests that the stability of synchronous states can be improved by making the generators homogeneous. Here, we show that a substantial additional improvement is possible by instead making the generators suitably heterogeneous. We develop a general method for attributing this counterintuitive effect to *converse symmetry breaking*, a recently established phenomenon in which the system must be asymmetric to maintain a stable symmetric state. These findings constitute the first demonstration of converse symmetry breaking in real-world systems, and our method promises to enable identification of this phenomenon in other networks whose functions rely on behavioral homogeneity.

¹Department of Physics and Astronomy, Northwestern University, Evanston, IL, USA. ²Northwestern Institute on Complex Systems, Northwestern University, Evanston, IL, USA. ³Present address: SimpleRose Inc, 1017 Olive Street, Suite 800, Saint Louis, MO 63101, USA. email: t-nishikawa@northwestern.edu

In an alternating current power grid, the generators provide electrical power that oscillates in time as sinusoidal waves. As these waves are superimposed before reaching the consumers, they need to be synchronized to the same frequency; otherwise, time-dependent cancellation between these waves would cause the delivered power to fluctuate, which can lead to equipment malfunction and damage¹. Maintaining frequency synchronization is challenging because the system is complex in various ways, with every generator responding differently to the continual influence of disturbances and varying conditions². Adding to the challenge is the increase in perturbations resulting from the ongoing integration of energy from intermittent sources³, the emergence of grid-connected microgrids⁴, and the expansion of an increasingly open electricity market⁵. Furthermore, the inherent heterogeneities in the parameters of system components and in the structure of the interaction network are perceived as obstacles to achieving synchronization. Consistent with the view that heterogeneities may generally inhibit frequency homogeneity, an earlier study showed that homogenizing the (otherwise heterogeneous) values of generator parameters can lead to stronger stability of synchronous states than in the original system⁶. An outstanding question remains, however, as to whether there is a heterogeneous parameter assignment (different from the nominal one) that would enable even stronger stability for synchronous states than the best homogeneous parameter assignment. Though motivated by its significance for power grids, this question is broadly relevant for improving the stability of homogeneous dynamics in complex network systems in general, including consensus dynamics in networks of human or robotic agents^{7,8}, coordinated spiking of neurons in the brain^{9,10}, and synchronization in communication networks^{11,12}.

To gain insights into the potential role of heterogeneity in enhancing stability, it is instructive to first consider the case of damped harmonic oscillators. For a single oscillator, the optimal stability corresponds to the fastest convergence to the stable equilibrium and is achieved when the oscillator is critically damped: underdamping would lead to lingering oscillations around the equilibrium, and overdamping would lead to slowed convergence due to excess dragging. This optimization is exploited in door closers (devices that passively close doors in a controlled manner), which are designed to be critically damped for the door to close fast without slamming. When multiple damped oscillators are coupled, the damping giving rise to optimal stability will be influenced by the network interactions. More important, we can show that the optimal stability in such a network requires different oscillators to have different damping (even when their other parameters are all identical and they are positioned identically in the network), as illustrated in Fig. 1.

In this paper, we first demonstrate that an analogous effect occurs in power-grid networks: heterogeneity in generator parameters can robustly enhance both the linear and the non-linear stability of synchronous states in power grids from North America and Europe. Since these systems have heterogeneity in the network structure in addition to the tunable generator parameters, one possibility is that the effect arises entirely from compensation: stability reduction due to one heterogeneity is compensated by another heterogeneity, leading to a stability enhancement when the latter heterogeneity is added. An alternative, which we validate here, involves the recently established phenomenon of *converse symmetry breaking* (CSB)¹³, in which the stability of a symmetric state requires the system's symmetry to be broken. Owing to its counterintuitive nature, this phenomenon had not been recognized until it was recently predicted and experimentally confirmed^{13,14} for synchronization in oscillator networks (a class of network

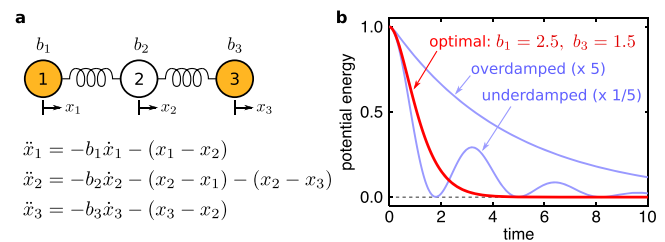


Fig. 1 Stabilizing effect of heterogeneity in a mass-spring system.

a System consisting of a linear chain of three unit masses connected by two identical springs. The masses are constrained to move horizontally, and their dynamics are governed by the equation shown, where x_i is the displacement of mass i relative to its equilibrium and b_i is its damping coefficient. **b** Total potential energy of the springs vs. time for three different damping scenarios. The optimal damping (red), corresponding to the fastest energy decay, is achieved for $b_1 = 2.5$, $b_2 = 3.2$, and $b_3 = 1.5$ (or, equivalently, $b_1 = 1.5$, $b_2 = 3.2$, and $b_3 = 2.5$), despite the fact that masses 1 and 3 are otherwise identical and identically coupled. Overdamping leads to a slower monotonic decay, while underdamping results in a slower oscillatory decay, as shown in blue by varying b_1 and b_3 by a factor of 5. In all cases, the initial conditions are $(x_1, x_2, x_3) = (1, 0, -1)$ and $(\dot{x}_1, \dot{x}_2, \dot{x}_3) = (0, 0, 0)$.

dynamics widely studied in the literature^{15–17}). Despite its conceptual generality and potential to underlie symmetric states of many systems, this phenomenon has not yet been observed outside laboratory settings. The symmetry relevant here is node-permutation symmetry, since in a synchronized state the states of different nodes are equal and can be permuted without altering the state of the system. For power grids, CSB would translate to a stability enhancement mechanism in which maintaining the stability of synchronous (and thus symmetric) states requires the generator parameters to be heterogeneous (thus making the system asymmetric). By systematically removing all the other system heterogeneities and isolating the effect of the generator heterogeneity, we establish that CSB is responsible for a significant portion of the stability improvement observed in the power grids we consider. This offers insights into mechanisms underlying the parameter heterogeneity that arises when the generators are tuned to damp oscillations^{18,19} (e.g., by adjusting devices called power system stabilizers). Our results are of particular relevance given that CSB has thus far not been observed in any real-world system outside controlled laboratory conditions, let alone power-grid networks.

Results

Power-grid dynamics and stability. To describe the dynamics of n generators in a power-grid network, we represent each generator node as a constant voltage source behind a reactance (the so-called classical model) and their interactions through intermediate non-generator nodes as effective impedances (a process known as Kron reduction)²⁰. We assume that the system is operating near a synchronous state in which the voltage frequencies of the n generators are all equal to a constant reference frequency ω_s , and we examine whether the homogeneous state is stable against dynamical perturbations. Such perturbations, whether they are small or large, may come for instance from sudden changes in generation and/or demand due to shifting weather condition at wind or solar farms, variations in power consumption, switching on/off connections to microgrids, etc. The short-term dynamics (of the order of one second or less) are then governed by the so-called swing

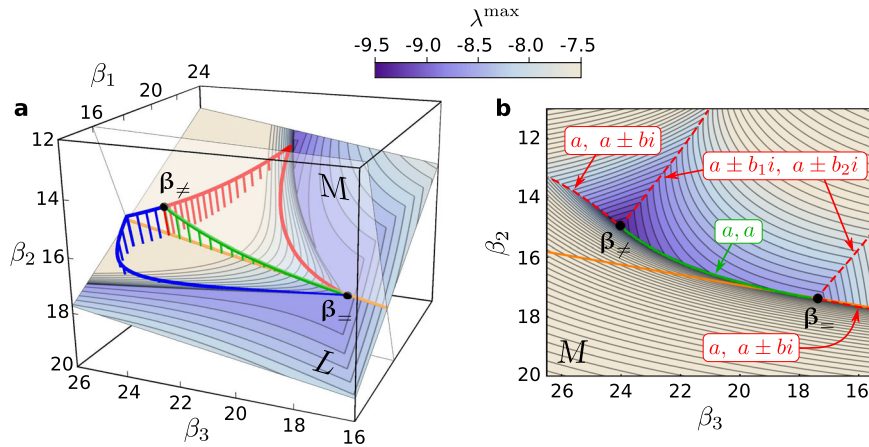


Fig. 2 Enhancing the stability of the 3-generator system along curved paths. **a** Examples of curved paths (red, green, and blue) in the β -space from β_+ to β_- along which the Lyapunov exponent λ^{\max} decreases monotonically. The numerically generated curves confirm our theoretical prediction that these paths are all tangent to the plane L at the point β_- . The droplines indicate that these curves are outside L . The contour levels of λ^{\max} are shown on L . Also shown is the plane M , which is defined as the plane perpendicular to L that contains β_- and β_+ . **b** Contour levels of λ^{\max} on the plane M , which contains the green path from **a**. The orange lines in **a** and **b** indicate the intersection between planes L and M . The red dashed curves (and the green path) trace cusp surfaces associated with degeneracies of the real parts of the eigenvalues of \mathbf{J} that determine λ^{\max} . Three types of degeneracy are indicated: a real eigenvalue equal to the real parts of a pair of complex conjugate eigenvalues ($a, a \pm bi$), two different complex conjugate eigenvalues with equal real parts ($a \pm b_1i, a \pm b_2i$), and two equal real eigenvalues (a, a). For details on the system, see “Methods”.

equation^{20,21}:

$$\ddot{\delta}_i + \beta_i \dot{\delta}_i = a_i - \sum_{k \neq i} c_{ik} \sin(\delta_i - \delta_k - \gamma_{ik}), \quad (1)$$

where δ_i is the phase angle variable for generator i (representing the generator’s internal electrical angle, relative to a reference frame rotating at the reference frequency ω_s); $\beta_i \equiv D_i/(2H_i)$ is an effective damping parameter (corresponding to b_i in the mass-spring system of Fig. 1), with constant D_i capturing both mechanical and electrical damping and constant H_i representing the generator’s inertia; a_i is a parameter representing the net power driving the generator (i.e., the mechanical power provided to the generator, minus the power demanded by the network, including loss due to damping); and c_{ik} and γ_{ik} are respectively the coupling strength and phase shift characterizing the electrical interactions between the generators. The parameters in Eq. (1) for a given system are determined by computing the active and reactive power flows between network nodes from system data and using them to calculate the complex-valued effective interaction (and thus its magnitude c_{ik} and angle γ_{ik}) between every pair of generators. In real power grids, stable system operation is ensured by a hierarchy of controllers that adjust generator power outputs and thus the parameters in Eq. (1). Here, however, these parameters can be regarded as constants, since the lowest level of control (known as the primary control) is modeled as a damping-like effect captured by the β_i term in Eq. (1), while the upper-level controls (known as the secondary and tertiary controls) act on time scales much longer than that of the short-term generator dynamics described by the model. In addition, fluctuations in power generation and demand on the time scales of minutes or longer (which can come, e.g., from renewable energy sources) do not affect the short-term dynamics. Equation (1) has recently been studied extensively in the network dynamics community^{3,6,22–25}.

We first analyze the stability of the synchronous state against small perturbations. The synchronous state corresponds to a fixed point of Eq. (1) given by $\delta_i = \delta_i^*$ and $\dot{\delta}_i = 0$, which represents frequency synchronization because $\dot{\delta}_i$ is the frequency relative to

the reference ω_s . The Jacobian matrix of Eq. (1) at this point can be written as

$$\mathbf{J} = \begin{pmatrix} \mathbf{O} & \mathbf{I} \\ -\mathbf{P} & -\mathbf{B} \end{pmatrix}, \quad (2)$$

where \mathbf{O} and \mathbf{I} denote the $n \times n$ null and identity matrices, respectively; $\mathbf{P} = (P_{ik})$ is the $n \times n$ matrix defined by

$$P_{ik} = \begin{cases} -c_{ik} \cos(\delta_i^* - \delta_k^* - \gamma_{ik}), & i \neq k, \\ -\sum_{k' \neq i} P_{ik'}, & i = k, \end{cases} \quad (3)$$

which expresses the effective interactions between the generators; and \mathbf{B} is the $n \times n$ diagonal matrix with β_i as its diagonal elements. We note that, while the form of the Jacobian matrix for coupled damped harmonic oscillators is the same as in Eq. (2), power grids are different in that they can have $\mathbf{P} \neq \mathbf{P}^T$ because $c_{ik} \neq c_{ki}$ in general and because γ_{ik} appears in Eq. (3). The stability under noiseless conditions is determined by the Lyapunov exponent defined as $\lambda^{\max} \equiv \max_{i \geq 2} \text{Re}(\lambda_i)$, where λ_i are the eigenvalues of \mathbf{J} . The identically zero eigenvalue, which comes from the zero row-sum property of \mathbf{P} and is denoted here by λ_1 , is excluded because it is associated with the invariance of the equation under uniform shift of phases. If $\lambda^{\max} < 0$, then the synchronous state is asymptotically stable, and smaller λ^{\max} implies stronger stability (this is known as small-signal stability analysis in power system engineering). Since real power-grid dynamics are noisy due to power generation/demand fluctuations and various other disturbances occurring on short time scales, λ^{\max} needs to be sufficiently negative to keep the system close to the synchronous state. Indeed, a previous study¹⁴ showed that, for broad classes of noise dynamics, there is a (negative) threshold value of λ^{\max} for such stability: the system is stable if and only if λ^{\max} is below the threshold. This stability threshold depends on the noise intensity level. For impulse-like disturbances, the intensity level corresponds to the maximum deviation of δ_i that can be induced by a single disturbance, such as a sudden loss of a generator or a spike in power demand. For continual disturbances, the intensity level can be quantified by the variances of the fluctuating power generation and demand, which can be modeled by adding a randomly varying term to the parameter a_i .

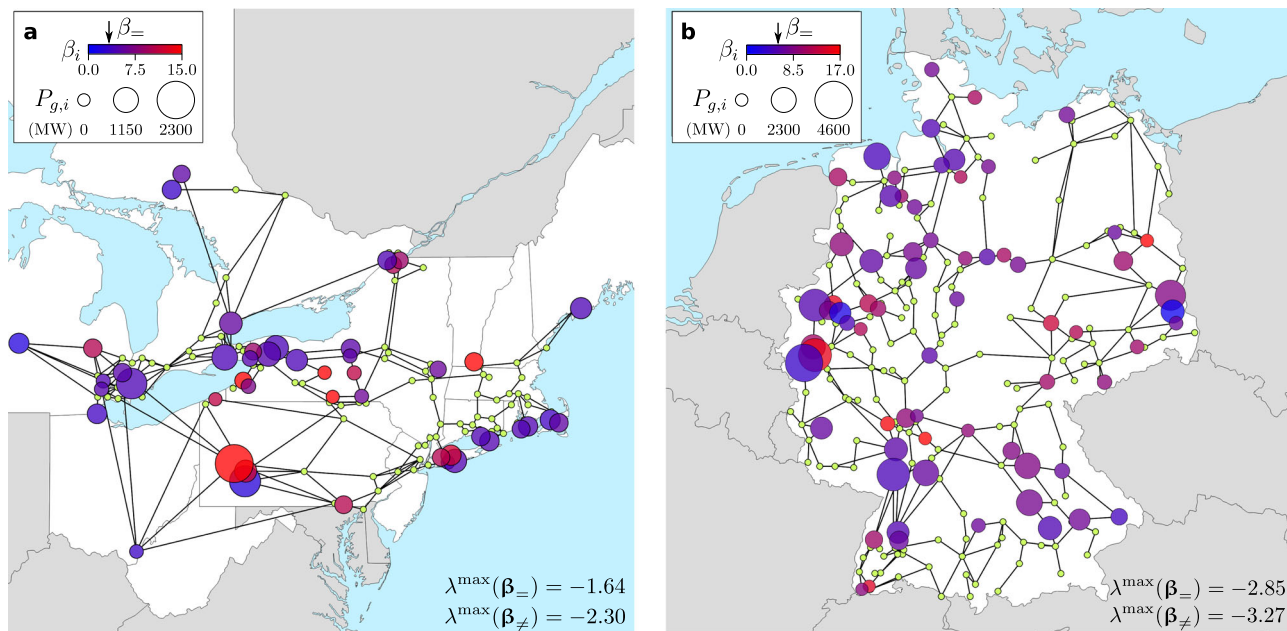


Fig. 3 Heterogeneity of optimized generator parameters β_i for two power grids. **a** Portion of the North American power grid corresponding to the former Northeast Power Coordinating Council (NPCC) region. **b** German portion of the European power grid. In both panels, a color-coded circle represents a generator or an aggregate of generators (see “Methods” for the aggregation procedure used), with the color indicating the corresponding optimal β_i in the vector β_{\neq} . The arrows above the color bars indicate $\beta_{=}$, the optimal uniform value of β_i . The λ^{\max} values for the uniform and non-uniform optimal β_i (in the vectors $\beta_{=}$ and β_{\neq} , respectively) are indicated at the bottom of each panel. The radius of the circle is proportional to the real power output of the generator in megawatts (MW). Small green dots indicate non-generator nodes. Details on these systems, including data sources, can be found in “Methods”.

Since the stability threshold is generally lower for higher noise levels, the lower the value of λ^{\max} for a given power grid, the more intense disturbances and fluctuations the system can endure without losing stability. Incidentally, the optimal damping in the mass-spring system of Fig. 1 is given precisely by minimizing λ^{\max} for that system.

Enhancing stability with generator heterogeneity. We now study $\lambda^{\max} = \lambda^{\max}(\beta)$ as a function of $\beta \equiv (\beta_1, \dots, \beta_n)$ for a selection of power grids whose dynamics can be described by Eq. (1) with the parameter values based on data. Using the same model, it was previously shown⁶ that, under the constraint that all β_i 's have the same value, λ^{\max} is minimized when $\beta = \beta_{=}$, where $\beta_{=} \equiv (\beta_{=}, \dots, \beta_{=})$ and $\beta_{=} \equiv 2\sqrt{\alpha_2}$, with α_2 denoting the smallest nonidentically zero eigenvalue of matrix \mathbf{P} . The eigenvalue α_2 is associated with the least stable eigenmode, and we assume that it is real and positive (as confirmed in all systems we consider). It was further shown that, at this homogeneous optimal point $\beta_{=}$, the function $\lambda^{\max}(\beta)$ is non-differentiable (which precludes the use of a standard derivative test), but its one-sided derivative along any given straight-line direction is positive, i.e., the directional derivative $D_{\beta'} \lambda^{\max}(\beta_{=})$ is positive in the direction of any n -dimensional vector β' . Thus, moving away from $\beta_{=}$ along any straight line would necessarily increase λ^{\max} from the local minimum value $\lambda^{\max}(\beta_{=}) = -\sqrt{\alpha_2}$ and hence only reduce the stability of the synchronous state.

Despite the apparent impossibility of improving on $\lambda^{\max}(\beta_{=})$ locally, we first show that there can be curved paths starting at $\beta_{=}$ along which λ^{\max} can be further minimized with heterogeneous β_i . Indeed, Fig. 2a illustrates using a 3-generator system that such curved paths exist and can connect $\beta_{=}$ to the (unique) global minimum, which we denote by β_{\neq} as its components are all different. The corresponding optimal $\lambda^{\max}(\beta_{\neq}) \approx -9.41$ represents more than 8% improvement over $\lambda^{\max}(\beta_{=}) \approx -8.69$. In

general, if a curved path starts at $\beta_{=}$, and if λ^{\max} decreases monotonically along that path, then it cannot be oriented in an arbitrary direction in the β -space. We show that it needs to be tangent to a system-specific plane (or hyperplane of co-dimension one for $n > 3$), denoted here by L and defined by the equation $\sum_{i=1}^n u_i v_i \beta_i = 0$, where u_i and v_i are the i th component of the left and right eigenvectors, respectively, associated with the eigenvalue α_2 . This result, illustrated by the three example paths in Fig. 2a, follows from the derivation of a formula for λ^{\max} and the full analytical characterization of the stability landscape near $\beta_{=}$ (both presented in Supplementary Note 1).

The curved paths of decreasing λ^{\max} are part of the complex structure of the stability landscape. These paths generally lie on a cusp surface, defined by the property that, at any point on the surface, λ^{\max} is non-differentiable and locally minimum along any direction transverse to the surface. The three paths shown in Fig. 2a all lie on the same cusp surface, which contains both $\beta_{=}$ and β_{\neq} . The intersection between this cusp surface and the plane M (the one perpendicular to L) is the green path of monotonically decreasing λ^{\max} shown in Fig. 2. In fact, there are infinitely many different paths of decreasing λ^{\max} on this cusp surface. Of these paths, the red and blue paths shown in Fig. 2a share the additional property of being an intersection between pairs of cusp surfaces. Each of these paths consists of at least two parts that are intersections between different pairs of cusp surfaces, which explains the kinks observed in Fig. 2 as points at which the curve switches from one intersecting surface to another. In larger systems, we find that their higher-dimensional β -spaces are sectioned by many entangled cusp hypersurfaces associated with spectral degeneracies (as illustrated in Supplementary Fig. 2 using the four larger systems we will introduce below). Their intersections, which themselves form cusp hypersurfaces of lower dimensions, are expected to contain curved paths of monotonically decreasing λ^{\max} . The existence of kinks and cusp surfaces in the stability landscape, which makes numerical search

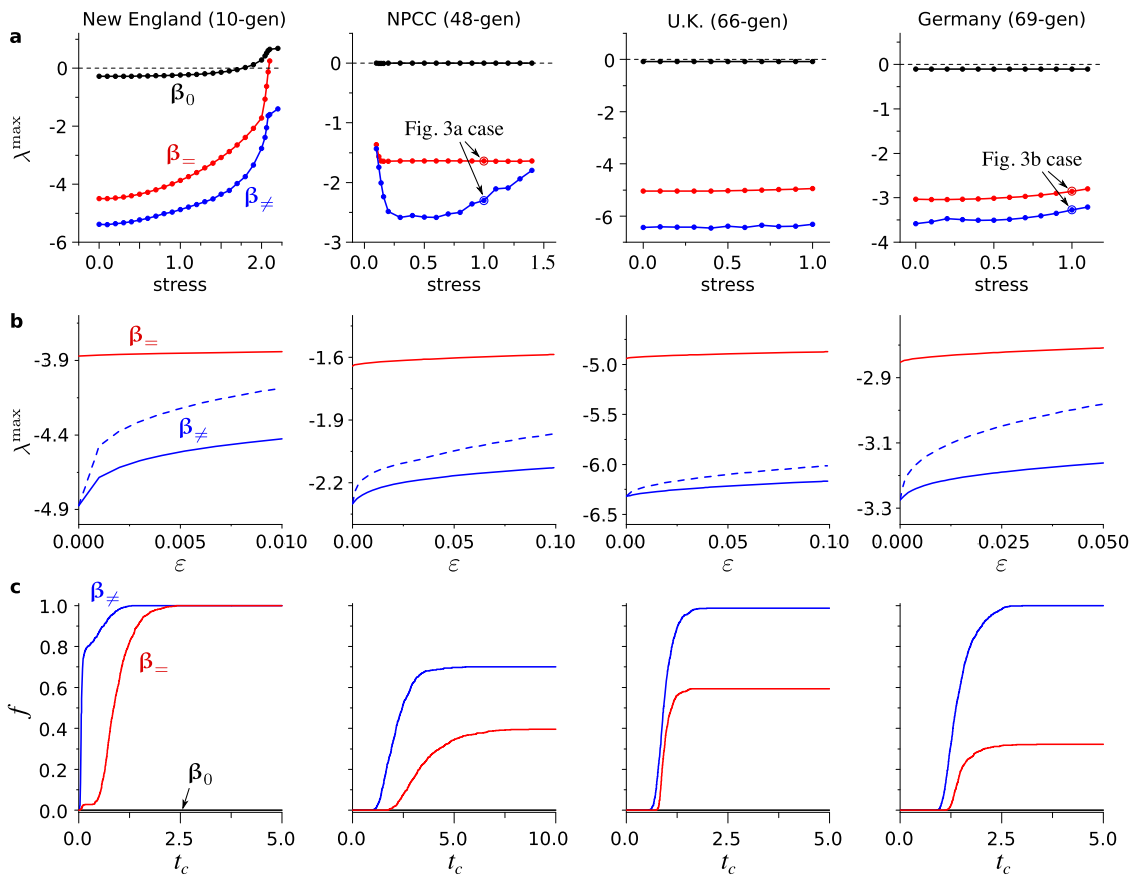


Fig. 4 Improving the stability of power grids with heterogeneity in β . The columns correspond to the four systems we consider. **a** Improved Lyapunov exponent λ^{\max} as functions of the system stress level for the heterogeneous optimum β_{\neq} (blue), the homogeneous optimum $\beta_{=}$ (red), and the original parameter β_0 (black). The cases shown in Fig. 3 are indicated in the second and the last plot. **b** Change of λ^{\max} under perturbations of size ϵ applied to β_{\neq} (blue). We show λ^{\max} as a function of ϵ , where solid and dashed curves indicate the average and the maximum, respectively, over perturbations in 1000 random directions. Note that the maximum corresponds to the worst case scenario. For comparison, we also show the average of λ^{\max} when $\beta_{=}$ is perturbed (red). **c** Fraction f of trajectories that converge to synchronous states before a given cutoff time t_c for β_{\neq} (blue), $\beta_{=}$ (red), and β_0 (black). Note that f for β_0 remains zero for all $t_c < 10$ seconds in all cases.

for global optima challenging, is not unique to power grids nor phase oscillator networks. It is a consequence of a much more general mathematical observation that the largest real part of the eigenvalues of a matrix (known as the spectral abscissa), such as λ^{\max} we consider here, is a non-smooth, non-convex, and non-Lipschitz function of the matrix elements²⁶.

Stabilizing heterogeneity in real power grids. Having established that heterogeneous β_{\neq} can improve stability over the homogeneous $\beta_{=}$ for a small example system, we now show that this result extends to much larger, real-world power grids. Specifically, we study the 48-generator NPCC portion of the North American power grid and the 69-generator German portion of the European power grid. Assessing the stability against small perturbations based on Eqs. (1)–(3) has the advantage of reducing the complexity of these systems to a single matrix \mathbf{P} and its eigenvalues. For each system, we identify a local minimum β_{\neq} that has heterogeneous β_i (and thus is distinct from $\beta_{=}$) and achieves the lowest λ^{\max} over 200 independent runs of simulated annealing. We find simulated annealing to be more effective than other methods in locating a minimum on a non-differentiable landscape²⁷. The resulting stability improvement over $\beta_{=}$ is substantial: $\lambda^{\max}(\beta_{=}) - \lambda^{\max}(\beta_{\neq}) = 0.66$ for the NPCC network and $\lambda^{\max}(\beta_{=}) - \lambda^{\max}(\beta_{\neq}) = 0.42$ for the German network. The optimized β_i assignment in β_{\neq} exhibits substantial heterogeneity

across each network and also across the corresponding geographical area (Fig. 3).

To validate the prevalence of such stability-enhancing heterogeneity, we also analyze λ^{\max} as a function of system stress level (to be precisely defined below) for four different systems, including the two used in Fig. 3 (see “Methods” for detailed descriptions of the systems and data sources). To increase or decrease the level of stress in a given system, we scale the power output of all generators and the power demand at all nodes by a common constant factor. We then re-compute the power flows across the entire network and the parameters of Eq. (1). The system stress level is then defined to be the common scaling factor used in this procedure. Thus, a stress level of 1 for a given system corresponds to the original demand level in the corresponding dataset. For each stress level, we estimate λ^{\max} at $\beta = \beta_{\neq}$ from 200 independent simulated annealing runs. Over the entire range of stress levels considered, we consistently observe a smaller λ^{\max} for β_{\neq} compared to $\beta_{=}$, the optimal homogeneous β_i assignment, and to β_0 , the original β_i assignment in the dataset (Fig. 4a).

To test the robustness of the identified optimal λ^{\max} against uncertainties in the β_i values, we study how λ^{\max} changes under perturbations along random directions in the β -space in the vicinity of β_{\neq} and (for comparison) in the vicinity of $\beta_{=}$. For the stress level of 1 and for each random direction, we compute λ^{\max} as a function of the perturbation size ϵ , measured in 2-norm. The resulting statistics from 1000 random directions indicate that, for

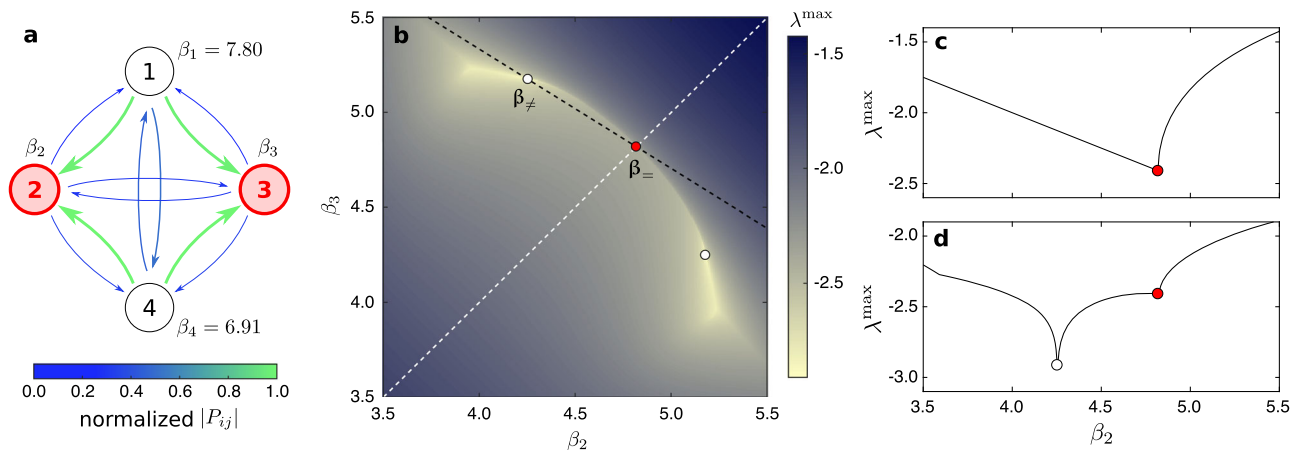


Fig. 5 Illustrating CSB in a 4-generator example system. **a** Effective interaction network connecting the generators and given by matrix \mathbf{P} . Both the thickness and color of the arrow connecting node j to node i represent the interaction strength $|P_{ij}|$, with the thickness proportional to $|P_{ij}|$ and the color encoding $|P_{ij}|$ normalized by its maximum over all i and j with $i \neq j$. **b–d** Dependence of λ^{\max} on β_2 and β_3 , with the values of β_1 and β_4 set to the values indicated in **a**. In **b**, λ^{\max} is color-coded to visualize the full 2D landscape. In **c**, λ^{\max} is shown as a function of β_2 along the white dashed line in **b**, corresponding to $\beta_2 = \beta_3$. It attains its minimum value ≈ -2.40 at $\beta_2 = \beta_3 \approx 4.80$ (red circle). In **d**, λ^{\max} as a function of β_2 along the black dashed line in **b** attains its minimum value ≈ -2.97 at $(\beta_2, \beta_3) \approx (4.27, 5.17)$ (white circle). Thus, the substantially improved optimal λ^{\max} is possible only when the permutation symmetry between generators 2 and 3 is broken. For details on the system, see “Methods”.

each system, there is a sizable neighborhood of the optimum β_x in which λ^{\max} is significantly lower than at β_+ , representing a stability improvement against small perturbations (Fig. 4b).

To show that the improvement is also observed for stability against large perturbations, we define a generalized notion of attraction basin as a set of initial conditions whose corresponding trajectories satisfy a criterion for convergence to synchronous states (a variation of the so-called basin stability²⁸). Here, the convergence criterion we use is that the instantaneous frequency enters into a narrow band around ω_s (within ± 0.3 Hz) and remains inside the band until $t_{\max} = 10$ seconds. This criterion is similar to what is typically used for transient stability analysis in power system engineering. It also captures a variety of synchronous states, including not only those corresponding to fixed points of Eq. (1) (with constant phase angle differences), but also those corresponding to time-dependent solutions of Eq. (1). To account for large perturbations, we consider initial conditions with arbitrary phase angles and frequencies within 1 Hz of the nominal frequency (60 Hz for the New England and NPPC systems; 50 Hz for the U.K. and German systems). Each initial condition can be regarded as resulting from a large impulse-like disturbance, such as a disconnection of a significant portion of the grid or a system-wide demand surge. The size of the basin can then be quantified using the fraction f of the corresponding trajectories that converge before a given cutoff time t_c , i.e., the fraction of those that satisfy $|\delta_i(t)|/(2\pi) \leq 0.3$ Hz for all $t \in [t_c, t_{\max}]$. For each t_c , the fraction f is estimated using 1000 initial conditions sampled randomly and uniformly from all states satisfying the criteria described above. As shown in Fig. 4c, we find that the estimated f is significantly larger for β_x than for β_+ (which in turn is much larger than for β_0). This indicates that the likelihood for the system to return to stable operation after a large disturbance is higher for the heterogeneous optimal β_i than for the homogeneous optimal ones. We also observe that larger systems tend to exhibit larger increase in the size of the asymptotic basins (i.e., in the value of f for $t_c \rightarrow \infty$).

Isolating converse symmetry breaking. Since real power systems generally have heterogeneity in a_i , c_{ik} , and γ_{ik} , the stability improvement enabled by the β_i heterogeneity (and the associated

system asymmetry) could in principle be a compensation for heterogeneity in the network structure, power demand and generation, or other component parameters (and the associated system asymmetries). To illustrate that no such compensation is needed and that CSB can be responsible for stability improvement, we use an example system consisting of four generators connected to each other and to one load (see Supplementary Fig. 1 for a system diagram). This system is symmetric with respect to the permutation of generators 2 and 3 if $\beta_2 = \beta_3$, and this symmetry is reflected in the property that $P_{2j} = P_{3j}$ for all j in the corresponding interaction matrix \mathbf{P} (Fig. 5a). The minimum λ^{\max} possible for this symmetric system is $\lambda^{\max} \approx -2.40$, which can be decreased further by $>20\%$ to $\lambda^{\max} \approx -2.97$ if the $\beta_2 = \beta_3$ constraint is lifted (Fig. 5b–d). This demonstrates CSB for this system under a range of noise levels: breaking the system’s symmetry under the permutation of generators 2 and 3 is required for λ^{\max} to cross the stability threshold and make the (symmetric) synchronous state stable. We note that the observation of CSB depends on the system’s symmetry. While CSB is observed in this 4-generator system (with a two-generator permutation symmetry), we do not observe CSB in a variant of the system with the four-generator permutation symmetry. We also note that, while the optimal β_i assignment does not share the two-generator permutation of the system, the two-dimensional stability landscape does, and it features a pair of equally optimal assignments related to each other through the symmetry (Fig. 5b). It is instructive to compare this result with the mass-spring system in Fig. 1, where similar breaking of a permutation symmetry (between masses 1 and 3) for a symmetric landscape (where optimal b_1 and b_3 are necessarily different but can be swapped) is shown to underlie optimal damping.

Having established that β_i heterogeneity alone can enhance stability through CSB, we now introduce a systematic method to separate CSB from other mechanisms that involve interplays between multiple heterogeneities. For this purpose, we transform matrix \mathbf{P} for each system used in Fig. 4, which does not have a pairwise node permutation symmetry, to a slightly different matrix \mathbf{P}' that does have the symmetry. More precisely, for a given pair of nodes i_1 and i_2 , we define this symmetrized matrix \mathbf{P}' by $P'_{ij} = P'_{i_2j} \equiv (P_{ij} + P_{i_2j})/2$ for all $j \neq i_1$ nor i_2 , making it symmetric under the permutation of nodes i_1 and i_2 . To elucidate

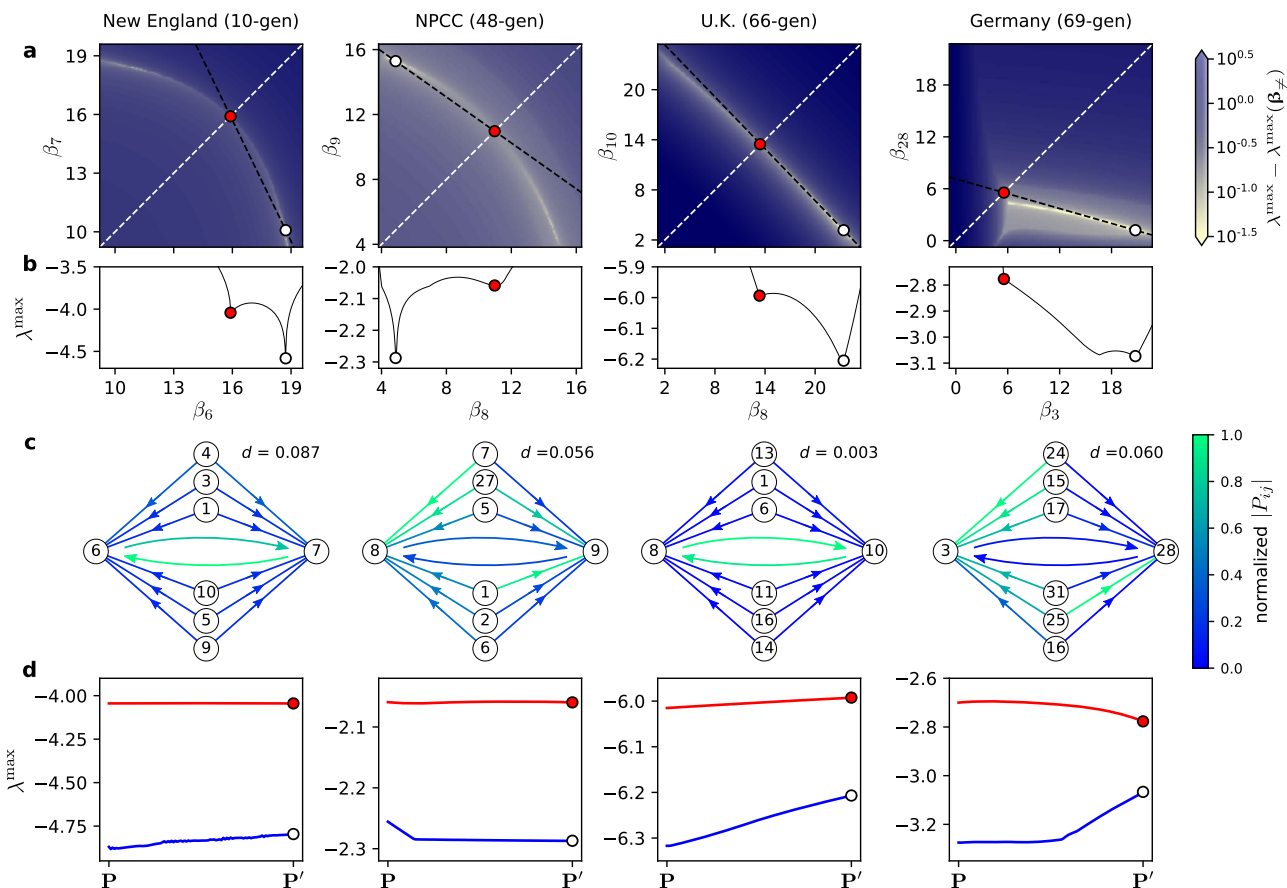


Fig. 6 Isolating the CSB effect in power grids. Each column synthesizes results for the system indicated at the top. **a** 2D stability landscape $\lambda^{\max}(\beta_{i_1}, \beta_{i_2})$, where i_1 and i_2 are the nodes whose permutation holds the symmetrized matrix \mathbf{P}' invariant. In each panel, the red circle marks the optimal $(\beta_{i_1}, \beta_{i_2})$ on the diagonal $\beta_{i_1} = \beta_{i_2}$ (white dashed line), while the white circle marks the optimal when $\beta_{i_1} \neq \beta_{i_2}$ is allowed. The other β_i are fixed at the values in β_{\neq} identified for a stress level of 1 in Fig. 4. **b** Stability λ^{\max} as a function of β_{i_1} along the black dashed line connecting the red and white circles in **a**, respectively. **c** Input strength patterns of the nodes i_1 and i_2 for the original matrix \mathbf{P} . The color of each arrow indicates $|P_{ij}|$, normalized by the largest value of $|P_{ij}|$ shown. For nodes i_1 and i_2 , we show incoming links from the top six common neighbors in terms of the input strength. Also shown is the distance d from the original matrix \mathbf{P} to its symmetrized version \mathbf{P}' , in which the two nodes receive identical incoming (weighted) links, defined as $d \equiv \|\mathbf{P} - \mathbf{P}'\|_2 / \|\mathbf{P}\|_2$, where $\|\cdot\|_2$ denotes the matrix 2-norm. **d** Change in the optimal λ^{\max} with (red) and without (blue) the constraint $\beta_{i_1} = \beta_{i_2}$, as we interpolate between the original matrix \mathbf{P} and its symmetrized version \mathbf{P}' . Node indexing for all four systems are described in “Methods”.

CSB for each system, we choose a node pair that simultaneously minimizes the difference between \mathbf{P} and \mathbf{P}' and maximizes the amount of stability improvement observed for \mathbf{P}' . For the four systems in Fig. 4, the stability of the symmetrized system can clearly be enhanced by allowing $\beta_{i_1} \neq \beta_{i_2}$, and much of the enhancement is maintained as one interpolates from the symmetrized system back to the original system (Fig. 6). This indicates that a significant portion of the stability enhancement for the original system can be attributed to CSB.

Discussion

Our demonstration that heterogeneity of generators can enhance the stability of synchronous states in a range of power grids suggests that there is large previously under-explored potential for tuning and upgrading current systems for better stability. Since larger conventional generators have larger inertia and thus larger impact on the stability of other generators, tuning of their parameters may be particularly beneficial. While we focused on the heterogeneity of a specific generator parameter here, further stability enhancement is likely to be possible by exploiting heterogeneity in other generator parameters and in the parameters of other network components as well as in the network topology. We suggest that such stability enhancement opportunities exist beyond power systems and may

extend to any network whose function benefits from homogeneous dynamics and whose stability depends on tunable system parameters. For example, the results presented here suggest that CSB can potentially be observed for coupled oscillatory flows in microfluidic networks and for networks of coupled chemical reactors whose oscillatory node dynamics is close to a Hopf bifurcation. It is known¹³ that such systems can be parameterized so that their Jacobian matrices take a form that generalizes Eq. (2) and thus is conducive to the emergence of CSB. The approach we developed here to isolate CSB is versatile and can be applied broadly to systems for which different heterogeneities co-occur. Determining how prevalent CSB is and how it depends on the properties of the system (e.g., the network size, link distribution, and node dynamics) are important questions for future research.

It is instructive to interpret our results and contrast them with past approaches in network optimization. In seeking the best approach, one may form two complementary hypotheses. One hypothesis, invoked in the past, was that the stability of the desired homogeneous states would be optimal when the system is homogeneous; the approach would thus be to limit the optimization search to the low-dimensional parameter subspace corresponding to networks with identical parameter values for all nodes. The other hypothesis, validated here, is that optimal stability of the desired homogeneous states is generally obtained

with heterogeneous parameter assignment, which implies that the search for this optimum requires exploring the high-dimensional parameter space without making a priori assumptions on how the parameters of different nodes are related. Recognizing this can lead to new control approaches designed to manipulate these parameters for further optimization of stability. We suggest that the fresh opportunities for network optimization and control revealed in this study apply to network systems in general and thus have the potential to inspire new discoveries in many different disciplines.

Methods

Power-grid datasets. Here, we describe the sources of data for the six power-grid networks considered (the 3-generator system in Fig. 2; the New England, NPCC, U.K., and German systems in Figs. 3, 4, and 6; and the 4-generator system in Fig. 5). For each system, the data provide the net injected real power at all generator nodes, the power demand at all non-generator nodes, and the parameters of all power lines and transformers. These parameters are sufficient to determine all active and reactive power flows in the system using a standard power flow calculation. The data also provide the generators' dynamic parameters H_i , D_i , and $x_{int,i}$ used in our stability calculations. The parameters H_i and D_i are the inertia and damping constants, respectively, that define the effective damping parameter through the relation $\beta_i = D_i/(2H_i)$. The parameter $x_{int,i}$ represents the internal reactance of generator i and is used in the calculation of the parameters a_i , c_{ij} , and γ_{ij} . In each system, nodes are indexed as in the original data source (except for the German power grid; see below).

- **3-generator test system (3-gen).** For this IEEE 3-generator, 9-node test system, which appeared in ref. 20, we used the data file (data3m9b.m) available in the PST toolbox²⁹. This system represents the Western System Coordinating Council (WSCC), which was part of the region now called the Western Electricity Coordinating Council (WECC) in the North American power grid. The data file provides all necessary dynamical parameters for each generator.
- **New England test system (10-gen).** For the IEEE 10-generator, 39-node test system, as described in refs. 30 and 31, we used the data file (case39.m) available in the MATPOWER toolbox³², with dynamic parameters added manually from ref. 30. This is a reduced model representing the New England portion of the Eastern Interconnection in the North American power grid, with one generator representing the connection to the rest of the grid.
- **NPCC power grid (48-gen).** For the 48-generator, 140-node NPCC power grid³³, we used the data file (data48em.m) available in the PST toolbox²⁹. The system represents the former NPCC region of the Eastern Interconnection in the North American power grid and includes an equivalent generator/load node representing the rest of the Interconnection. The data file provides H_i and $x_{int,i}$ for all generators (while it assumes $D_i=0$). We generated D_i randomly by sampling from the uniform distribution on the interval [1, 3] (in per unit on the system base, as specified by the data file). The geographic coordinates of the nodes used in Fig. 3a were extracted from ref. 34, and the coastline and boundary data used to draw the map were obtained from Natural Earth³⁵.
- **U.K. power grid (66-gen).** For the 66-generator, 29-node U.K. power grid, we used the data file (GBreducednetwork.m) available from ref. 36. The system represents a reduced model for the power grid of Great Britain. The dynamical parameters, H_i , D_i , and $x_{int,i}$, were generated randomly by sampling from the uniform distribution on the intervals, [1, 5], [1, 3], and [0.001, 0.101], respectively. The generated parameters values for each generator are in per unit on its own machine base, i.e., normalized by the reference values computed from the power base for the generator (chosen to be 1.5 times the maximum real power generation provided in the data file). For stability calculations, we converted these values to the corresponding values in per unit on a common system base.
- **German power grid (69-gen).** For the 69-generator, 228-node German power grid, we created the data from the ENTSO-E 2009 Winter model³⁷. The ENTSO-E model is a DC power flow model of the continental Europe and contains 1,486 nodes and 565 generators. We first created a dynamical model for the entire ENTSO-E network by solving the DC power flow and converting it to an AC power flow solution (assuming a 0.95 power factor at each node), and then generating dynamical parameters using the same method as for the U.K. grid. For any node with multiple generators attached, the net reactive power injection was distributed among these generators in proportion to their real power generation. From this full ENTSO-E model, we extracted the German portion by eliminating (using Kron reduction) all the nodes outside Germany (identified using the country label "D" representing Germany in the dataset). We re-indexed the extracted nodes consecutively, preserving the original ordering. The geographic coordinates of the nodes used in Fig. 3b were extracted from the PowerWorld data files available from ref. 37, and the coastline and boundary data used to draw the map were obtained from Natural Earth³⁵.

- **4-generator example system.** For the 4-generator, 5-node example system used in Fig. 5, we show a full system diagram in Supplementary Fig. 1, indicating the main parameters of the components. When the damping parameters of generators 2 and 3 are equal (i.e. $\beta_2 = \beta_3$), the system is symmetric under the permutation of these generators. MATLAB code for running simulations on this system, which includes the full set of parameters and uses the MATPOWER toolbox³², is available from our GitHub repository³⁸.

Aggregation of generators and effective damping parameter β_i . If a subset of generators are synchronized in the sense that $\delta_i - \delta_j$ is constant in time for any two generators i and j in the subset, then they can be represented by a single equivalent generator using a Zhukov-based aggregation method similar to that described in ref. 33. In this method, the equivalent generator has inertia constant $\sum_i H_i$ and damping constant $\sum_i D_i$, where the sums are taken over the generators i in the subset. The effective damping parameter of the equivalent generator is then $\sum_i D_i / (2 \sum_i H_i) = \bar{D} / (2 \bar{H})$, where \bar{D} and \bar{H} are respectively the average of the inertia and damping constants of the generators in the subset. Thus, the aggregation does not introduce any artificial heterogeneity.

Data availability

Data on all six systems we consider (described in "Methods") and detailed data of the core results presented in the figures are available from our GitHub repository³⁸.

Code availability

Essential code for reproducing the core results in all figures, as well as scripts for generating plain versions of the figures, is available from the GitHub repository³⁸.

Received: 26 August 2020; Accepted: 15 January 2021;

Published online: 05 March 2021

References

1. Machowski, J., Lubosny, Z., Bialek, J. W. & Bumby, J. R. *Power System Dynamics: Stability and Control* (John Wiley, Hoboken, 2020).
2. Backhaus, S. & Chertkov, M. Getting a grip on the electrical grid. *Phys. Today* **66**, 42–48 (2013).
3. Schäfer, B., Beck, C., Aihara, K., Witthaut, D. & Timme, M. Non-Gaussian power grid frequency fluctuations characterized by Lévy-stable laws and superstatistics. *Nat. Energy* **3**, 119–126 (2018).
4. Olivares, D. E. et al. Trends in microgrid control. *IEEE T. Smart Grid* **5**, 1905–1919 (2014).
5. Griffin, J. M. & Puller, S. L. eds. *Electricity Deregulation: Choices and Challenges* (University of Chicago Press, Chicago, 2009).
6. Motter, A. E., Myers, S. A., Anghel, M. & Nishikawa, T. Spontaneous synchrony in power-grid networks. *Nat. Phys.* **9**, 191–197 (2013).
7. Judd, S., Kearns, M. & Vorobeychik, Y. Behavioral dynamics and influence in networked coloring and consensus. *Proc. Natl Acad. Sci. USA* **107**, 14978–14982 (2010).
8. Ren, W. & Cao, Y. *Distributed Coordination of Multi-agent Networks* (Springer, London, 2010).
9. Axmacher, N., Mormann, F., Fernández, G., Elger, C. E. & Fell, J. Memory formation by neuronal synchronization. *Brain Res. Rev.* **52**, 170–182 (2006).
10. Penn, Y., Segal, M. & Moses, E. Network synchronization in hippocampal neurons. *Proc. Natl Acad. Sci. USA* **113**, 3341–3346 (2016).
11. Bregni, S. *Synchronization of Digital Telecommunications Networks* (John Wiley & Sons, West Sussex, 2002).
12. Wu, Y.-C., Chaudhari, Q. & Serpedin, E. Clock synchronization of wireless sensor networks. *IEEE Signal. Proc. Mag.* **28**, 124–138 (2010).
13. Nishikawa, T. & Motter, A. E. Symmetric states requiring system asymmetry. *Phys. Rev. Lett.* **117**, 114101 (2016).
14. Molnar, F., Nishikawa, T. & Motter, A. E. Network experiment demonstrates converse symmetry breaking. *Nat. Phys.* **16**, 351–356 (2020).
15. Arenas, A., Díaz-Guilera, A., Kurths, J., Moreno, Y. & Zhou, C. Synchronization in complex networks. *Phys. Rep.* **469**, 93–153 (2008).
16. Kiss, I. Z., Rusin, C. G., Kori, H. & Hudson, J. L. Engineering complex dynamical structures: sequential patterns and desynchronization. *Science* **316**, 1886–1889 (2007).
17. Matheny, M. H. et al. Exotic states in a simple network of nanoelectromechanical oscillators. *Science* **363**, eaav7932 (2019).
18. Rogers, G. *Power System Oscillations* (Springer Science & Business Media, New York, 2012).
19. Obaid, Z. A., Cipcigan, L. M. & Muhssin, M. T. Power system oscillations and control: classifications and PSSs' design methods: a review. *Renew. Sust. Energ. Rev.* **79**, 839–849 (2017).

20. Anderson, P. M. & Fouad, A. A. *Power System Control and Stability* (IEEE Press, Piscataway, NJ, 2003).
21. Nishikawa, T. & Motter, A. E. Comparative analysis of existing models for power-grid synchronization. *New J. Phys.* **17**, 015012 (2015).
22. Susuki, Y., Mezić, I. & Hikiyama, T. Coherent swing instability of power grids. *J. Nonlinear Sci.* **21**, 403–439 (2011).
23. Menck, P. J., Heitzig, J., Kurths, J. & Schellnhuber, H. J. How dead ends undermine power grid stability. *Nat. Commun.* **5**, 3969 (2014).
24. Yang, Y. & Motter, A. E. Cascading failures as continuous phase-space transitions. *Phys. Rev. Lett.* **119**, 248302 (2017).
25. Schäfer, B., Witthaut, D., Timme, M. & Latora, V. Dynamically induced cascading failures in power grids. *Nat. Commun.* **9**, 1–13 (2018).
26. Burke, J. V. & Overton, M. L. Variational analysis of non-Lipschitz spectral functions. *Math. Programming* **90**, 317–351 (2001).
27. Nishikawa, T., Molnar, F. & Motter, A. E. Stability landscape of power-grid synchronization. *IFAC-PapersOnLine* **48**, 1–6 (2015).
28. Menck, P. J., Heitzig, J., Marwan, N. & Kurths, J. How basin stability complements the linear-stability paradigm. *Nat. Phys.* **9**, 89–92 (2013).
29. Chow, J. H. & Cheung, K. W. A toolbox for power system dynamics and control engineering education and research. *IEEE Trans. Power Syst.* **7**, 1559–1564 (1992).
30. Pai, M. *Energy Function Analysis for Power System Stability* (Kluwer Academic Publishers, Norwell, 1989).
31. Athay, T., Podmore, R. & Virmani, S. A practical method for the direct analysis of transient stability. *IEEE Trans. Power Appar. Syst.* **PAS-98**, 573–584 (1979).
32. Zimmerman, R. D., Murillo-Sánchez, C. E. & Thomas, R. J. MATPOWER: steady-state operations, planning and analysis tools for power systems research and education. *IEEE Trans. Power Syst.* **26**, 12–19 (2011).
33. Chow, J. H. *Power System Coherency and Model Reduction* (Springer, New York, 2013).
34. Qi, J., Sun, K. & Kang, W. Optimal PMU placement for power system dynamic state estimation by using empirical observability Gramian. *2015 IEEE Power & Energy Society General Meeting* (Denver, CO, USA, 2015).
35. Patterson, T. & Kelso, N. V. *Natural Earth: Free Vector and Raster Map Data*, March 2018, <http://www.naturalearthdata.com/> (2018).
36. Bukhsh, W. A. & McKinnon, K. *Network Data of Real Transmission Networks*, April 2013, <https://www.maths.ed.ac.uk/optenergy/NetworkData/reducedGB> (2013).
37. Hutcheon, N. & Bialek, J. W. Updated and validated power flow model of the main continental European transmission network. *2013 IEEE Grenoble Conference*, Grenoble, France, p. 1–5. Data files available at <http://www.powerworld.com/bialek> (2013).
38. Molnar, F., Nishikawa, T. & Motter, A. E. Asymmetry underlies stability in power grids (this paper), GitHub repository: code and data for analyzing converse symmetry breaking in power-grid networks, <https://doi.org/10.5281/zenodo.4437866> (2021).

Acknowledgements

The authors thank Alex Mercanti and Yuanzhao Zhang for insightful discussions. This research was supported by Northwestern University's Finite Earth Initiative (supported by Leslie and Mac McQuown) and ARPA-E Award No. DE-AR0000702 and benefited from logistical support provided by Northwestern University's Institute for Sustainability and Energy.

Author contributions

F.M., T.N., and A.E.M. designed the research, analyzed the results, and wrote the paper. F.M. performed the simulations. All authors approved the final manuscript.

Competing interests

The authors declare no competing interests.

Additional information

Supplementary information The online version contains supplementary material available at <https://doi.org/10.1038/s41467-021-21290-5>.

Correspondence and requests for materials should be addressed to T.N.

Peer review information *Nature Communications* thanks Benjamin Schäfer and the other, anonymous, reviewer(s) for their contribution to the peer review of this work.

Reprints and permission information is available at <http://www.nature.com/reprints>

Publisher's note Springer Nature remains neutral with regard to jurisdictional claims in published maps and institutional affiliations.



Open Access This article is licensed under a Creative Commons Attribution 4.0 International License, which permits use, sharing, adaptation, distribution and reproduction in any medium or format, as long as you give appropriate credit to the original author(s) and the source, provide a link to the Creative Commons license, and indicate if changes were made. The images or other third party material in this article are included in the article's Creative Commons license, unless indicated otherwise in a credit line to the material. If material is not included in the article's Creative Commons license and your intended use is not permitted by statutory regulation or exceeds the permitted use, you will need to obtain permission directly from the copyright holder. To view a copy of this license, visit <http://creativecommons.org/licenses/by/4.0/>.

© The Author(s) 2021